PROCEEDINGS OF SCIENCE

Magnetic field effects on UHECR propagation

Silvia Mollerach*

CONICET,
Centro Atómico Bariloche, Av. Bustillo 9500, Bariloche, Argentina

E-mail: mollerach@gmail.com

The magnetic fields in our Galaxy, in the intergalactic space and around cosmic ray sources have significant effects on the observed arrival direction distribution, spectrum and composition of the ultra-high energy cosmic rays observed at Earth. I revisit some selected topics regarding the propagation in the regular Galactic magnetic field and in turbulent extragalactic magnetic fields. These include the formation of multiple images and the modification of large-scale anisotropies of extragalactic origin by the Galactic field. The arrival direction distribution and enhancement of the flux from a source in the presence of a turbulent field is also discussed, as well as the magnetic horizon effect that limits the flux of low-energy particles from a distribution of sources. The role of these effects in scenarios proposed to explain the spectrum, composition and anisotropies is highlighted.

*7th International Symposium on Ultra High Energy Cosmic Rays (*UHECR2024*)*
17-21 November 2024
Malargüe, Mendoza, Argentina

*Speaker

ISSN 1824-8039 . Published by SISSA Medialab.

PoS(UHECR2024)002

1. Introduction

While cosmic rays (CR) travel from their sources to the Earth, they traverse magnetic fields that deflect their trajectories, both in the intergalactic space as well as within our Galaxy. The deflections are inversely proportional to the cosmic-ray energy and proportional to their charge. Thus, the smallest deflections are expected at the highest energies and for the lightest particles. Since cosmic magnetic fields are uncertain, we do not know the size of the deflections they suffer and whether their propagation is diffusive or quasi-rectilinear for each energy and charge. The deflections may significantly affect both the arrival directions and the spectrum of the particles reaching the Earth.

We suspect in fact that the effects of magnetic fields on cosmic rays are significant. On the one hand, the interpretation of the recent results on the spectrum and composition from the Pierre Auger Observatory indicates that above ~ 3 EeV cosmic rays become progressively heavier and with little admixture of masses at any given energy, what leaves little room for light particles at the highest energies, as can be seen in Fig. 1 [1,2].

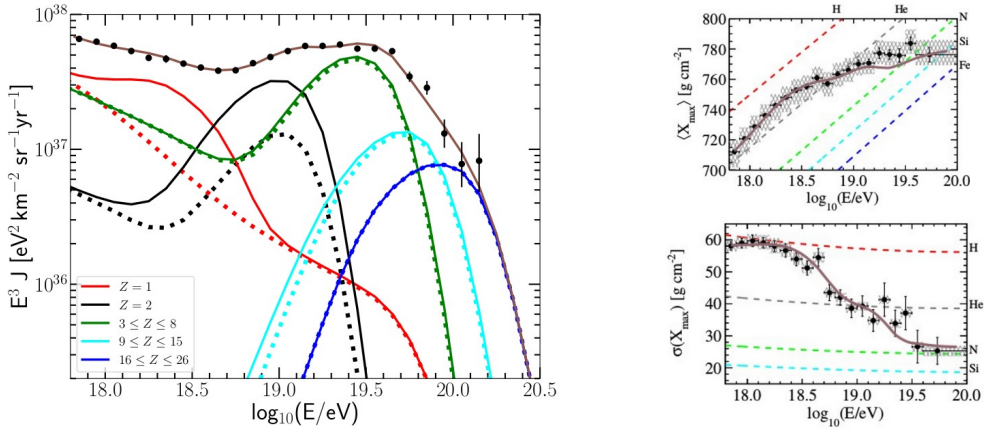

Figure 1: Interpretation of the spectrum and maximum depth of the showers (X_{max}) measurements by the Pierre Auger Collaboration for the EPOS-LHC hadronic interactions model [1,2].

On the other hand, anisotropy measurements have revealed a significant large-scale dipolar anisotropy with amplitude of 7.3% for energies above 8 EeV [3], some hints of intermediate scale anisotropies at angular scales of ~ 30° from the Cen A region with a significance of ~ 4 σ [4] and no evidence of anisotropies at small angular scales. These observations provide indications of the presence of large deflections in Galactic and/or extragalactic magnetic fields, compatible with the heavy composition inferred at the highest energies.

The main problem to identify the ultra-high energy cosmic ray (UHECR) sources is that both the Galactic and extragalactic magnetic fields are poorly known. The deflection of a particle of energy E a charge Z after traversing a distance L in a regular magnetic field $B(x)$ is given by

$$\delta \simeq 10^o \frac{EeV}{E/Z} \left| \int_0^L \frac{d\vec{x}}{kpc} \times \frac{\vec{B}}{2\mu G} \right|,$$

while the root mean square deflection in a turbulent magnetic field of root mean square amplitude B_{rms} and coherence length l_c is given by

$$\delta_{rms} \simeq \frac{B_{rms} Ze}{E} \sqrt{\frac{L\, l_c}{2}} \simeq 4^o \frac{B_{rms}}{nG} \frac{10\, EeV}{E/Z} \frac{\sqrt{L\, l_c}}{Mpc}.$$

Measuring magnetic fields in cosmic structures is difficult and different methods are used to gather information [5]. A widely used probe is the measurement of the Faraday rotation of the polarization of the radio emission from distant sources. The change in the polarization angle after traversing the foreground magnetized plasma is proportional to the integral of the magnetic field component along the line of sight times the electron density. Another complementary probe of cosmic magnetic fields is the diffuse radio synchrotron emission from the magnetized plasma. This emission is proportional to the integral of the square of the magnetic field component perpendicular to line of sight times the electron density.

The magnetic field in the Milky Way has been extensively studied analysing the Faraday rotation of pulsars in the Galaxy and other faraway sources and the synchroton emission from the Galactic medium. Although different groups have different models to account for the data, a consensus about some basic facts has been reached [6]. The Galactic magnetic field (GMF) has both a regular and a turbulent component, with amplitudes of about few μG. The regular field has several components: the disk one following different spiral arms, a halo component with toroidal shapes in the north and south Galactic hemispheres and an X component, named in this way because of the shape of the field lines observed when looking to the Galaxy edge-on. In addition to this component, the Galaxy has also a turbulent or random component with a similar or larger amplitude than the regular one, which is less well known. A discussion of recent GMF models is presented in [7,8].

Although there are not many measurements of magnetic fields in the cosmic structures, observations indicate that their strength strongly depend on the environment, with larger values in denser regions [9]. In collapsed structures such as galaxies and cluster centers, magnetic fields of a few μG have been inferred, while in cluster outskirts, 100 nG fields have been measured. Also filaments with a few tens of nG fields have been detected, and in voids, upper bounds $B \leq$ nG have been established. In recent years, there has been a huge computational effort to incorporate magnetohydrodynamics into large-scale structure formation simulations to understand the process of magnetogenesis. The magnetic fields result from the gravitational collapse compression and eventual dynamo processes and their amplitude depends on the generation mechanism of the initial seeds. These can be primordial, from processes taking place close to the Big Bang, like in inflation or early universe phase transitions before recombination. Alternatively (or additionally), they could arise from astrophysical processes taking place at low redshifts, e.g. star formation in galaxies and/or the formation of supermassive black holes which can expel magnetized plasma into the inter-galactic medium through galactic winds. Jets and winds from active galactic nuclei can also magnetize the central regions of clusters. Dynamo processes can further amplify the magnetic fields. These mechanisms can produce magnetic fields with strengths increasing with the matter overdensity and reaching the observed amplitudes in clusters [10].

2. Regular Galactic magnetic field effects on cosmic rays

The main effects of the regular GMF on cosmic rays reaching the Earth can be visualized in Fig. 2. It depicts the directions outside the halo of a regular grid of directions at Earth, obtained by backtracking antiparticles with rigidity E/Z = 20 EeV in the GMF model from Jansson and Farrar [11]. The mapping depends on the rigidity considered, with larger deformations taking place for smaller rigidities.

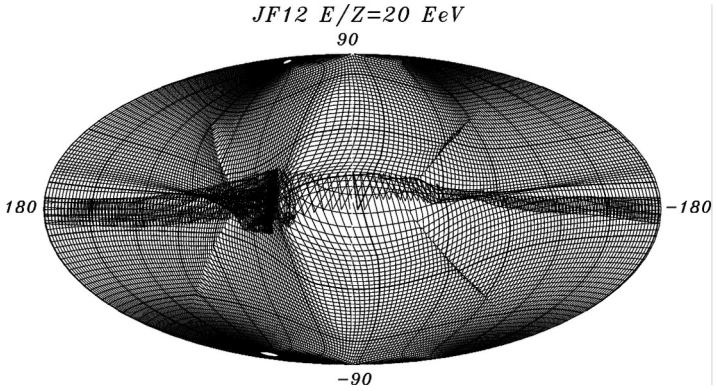

Figure 2: corresponding directions outside the halo for a regular grid of directions at Earth after propagation through the Jansson & Farrar Galactic magnetic field model.

Several features are evident in the figure. The deformation of the mapping indicates the deflections resulting for the different sky directions. In several places, folds appear in the map. This means that, in some cases, cosmic rays coming from the same direction outside the halo can arrive at Earth from different directions. This gives rise to multiple images of a source, which appear in different directions in the sky. Sources located in a region of the sky where the grid looks stretched will be demagnified, since the apparent solid angle at Earth is smaller than in the absence of the GMF and the surface brightness is conserved in the presence of magnetic deflections. On the contrary, sources located in regions where the grid is compressed will appear brighter, since the apparent solid angle at Earth is larger [12]. In particular, an isotropic distribution of equal-luminosity sources outside the halo will appear at Earth fainter and more dense in the regions where the grid looks stretched and brighter and more separated in the regions where the grid looks compressed. In the limit of an infinitely dim and dense population of sources, both effects cancel each other and an isotropic flux outside the halo is also isotropic at Earth after traversing the GMF, as expected from the Liouville theorem.

Different possible signatures of the regular GMF effects on the cosmic-ray flux can be expected to be observed. For instance, cosmic rays of the same mass composition coming from the same source should appear aligned in the sky and ordered in energy. These magnetic multiplets are expected to be detectable if there is a fraction of light cosmic rays at the highest energies. The Pierre Auger Collaboration has looked for them, with no significant detection [13], what is compatible with the inferred heavy composition at the highest energies.

The appearance of multiple images of a single source is actually a very plausible possibility even at very large energies, taking into account the composition inferred from the $X_{\rm max}$ measurements by Auger. Figure 3 displays the expected images of nitrogen cosmic rays

with energy of 20 EeV coming from a source at M82 (left) and at CenA (right) after traversing the GMF model of Jansson and Farrar [14].

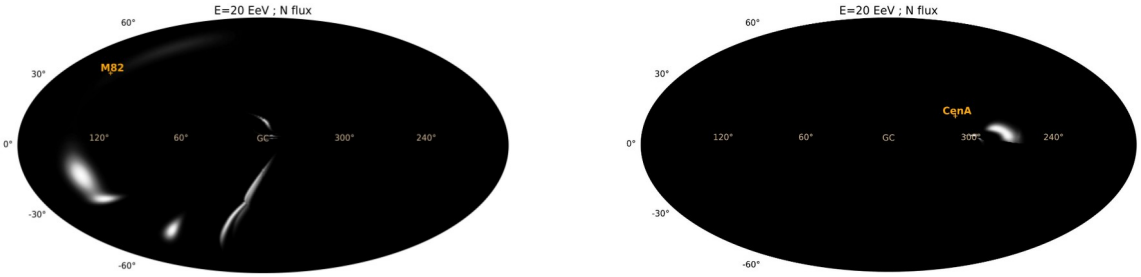

Figure 3: Images at Earth of a source of 20 EeV nitrogen cosmic rays in the direction of M82 (left panel) and Cen A (right panel) [14].

The GMF is also expected to have a significant effect on the large-scale anisotropy observations, changing the direction as well as the amplitude of the dipolar anisotropy measured at Earth with respect to that of the cosmic-ray flux outside the Galactic halo. As shown in Fig. 4, the deflections in the GMF tend to move the dipole direction closer to the outer or the inner spiral arm, depending on the original direction, and to decrease its amplitude for decreasing rigidities [15].

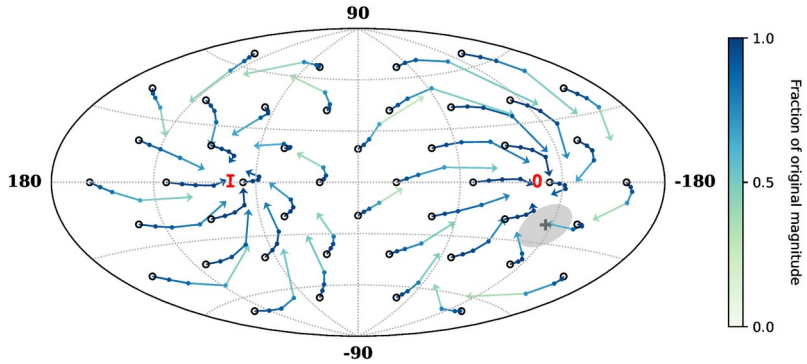

Figure 4: Dipolar component direction at Earth for different directions (black circles) of a perfect dipole outside the halo for different rigidities E/Z = 32, 16, 8 (intermediate points) and 4 EeV (tip of the arrow). The colors indicate the fractional decrease of the dipole amplitude for the Jansson and Farrar GMF model (from [15]).

3. Turbulent magnetic field effects on cosmic rays

A turbulent magnetic field also affects the distribution of arrival directions and spectrum of cosmic rays. Let us consider an isotropic turbulent field with root mean square amplitude $B_{\rm rms}$ and coherence length $l_{\rm c}$. There is a critical energy for which the Larmor radius of particles with energy $E_{\rm c}$ and charge Z equals the coherence length, $E_{\rm c} = ZeB_{\rm rms}l_{\rm c} = 0.9\ B_{\rm rms}\, l_{\rm c}/(\text{nG Mpc})$ EeV. For $E < E_{\rm c}$ particles will experience resonant diffusion, while for $E > E_{\rm c}$ they will experience small deflections within $l_{\rm c}$. After traversing a distance equal to the diffusion length $l_{\rm D}$ the particles are deflected by an angle of one radian. For a Kolmogorov spectrum one has that [16]

$$l_D(E) \simeq l_c \left[4\left(\frac{E}{E_c}\right)^2 + 0.9\left(\frac{E}{E_c}\right) + 0.23\left(\frac{E}{E_c}\right)^{1/3} \right].$$

The main characteristic of UHECRs trajectories in the presence of a turbulent magnetic field can be obtained by the numerical integration of a stochastic differential equation [17,16,18]

$$dn_i = (1/l_D)\, n_i\, c\, dt + (1/\sqrt{l_D})\, P_{ij}\, dW_j ,$$

where $P_{ij} \equiv \delta_{ij} - n_i n_j$ is the projection tensor onto the plane orthogonal to the direction of the CR velocity $\hat{n} \equiv (n_1, n_2, n_3)$ and (dW_1, dW_2, dW_3) are three Wiener processes such that $\langle dW_i \rangle = 0$ and $\langle dW_i\, dW_j \rangle = c\, dt\, \delta_{ij}$.

Cosmic rays from a single source will reach the observer from a set of directions around the source location, with an increasing spreading for decreasing rigidities. At high rigidities a single, slightly displaced image appears, while new multiple images start to appear for decreasing rigidities, leading to an increasingly blurred image. For low rigitidies, the distribution of directions is well described by a Fisher distribution $dN/d\cos\theta \propto \exp(\kappa(R)\cos\theta)$, with θ the angle between the source direction and the CR arrival direction [19]. The left panel of Fig. 5 shows the angular distribution of arrival directions for three values of the ratio between the distance to the source r_s and the difussion length, $R \equiv r_s/l_D$, where the transitions between a more concentrated image for low R to a more dipolar-like one for large R can be seen. The dots correspond to the integration of the stochastic differential equation. The concentration parameter κ determines the dispersion of the directions, with larger values corresponding to smaller dispersion. It is a decreasing function of the ratio R, as shown in the top right panel of Figure 5.

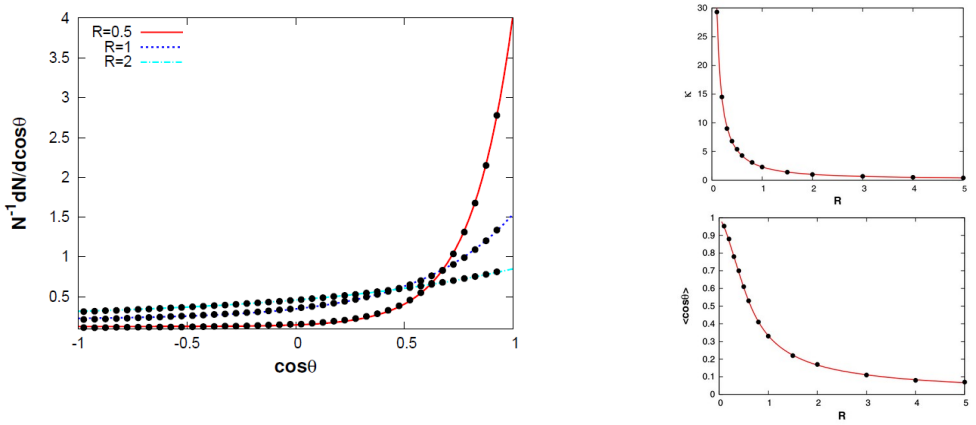

Figure 5: Distribution of arrival directions from a single source for different values of the ratio between the source distance and the diffusion length, R (left). Concentration parameter (top right) and mean $\cos\theta$ (bottom right) as a function of R [19].

The dipolar component of the distribution can be obtained from $\langle\cos\theta\rangle$ shown in the bottom left panel of Fig. 5 as $\Delta = 3\,\langle\cos\theta\rangle$. The fit shown corresponds to $\langle\cos\theta\rangle = (1 - \exp(-3R - 7R^2/2))/3R$, smoothly interpolating from $\Delta \simeq 3l_D/r_s$ in the diffusive regime (Fick's law) and $\Delta \simeq 3\,(1 - r_s/3l_D)$ in the ballistic regime, i.e. $\langle\theta^2\rangle \simeq 2r_s/3l_D \simeq (r_s/6L_c)(E/E_c)^2$ at large energies.

The turbulent magnetic field also affects the observed flux from a source. Let us first consider the case of a steady source, neglecting energy losses. The spatial density of CRs from the source will reach an asymptotic stationary regime in which it does not depend on time, and the flux through any sphere around the source has to be the same. Due to the spherical symmetry

$$n(E,r_s)\, 4\pi\, r_s^2 c\, \langle\cos\theta(E,r_s)\rangle = Q(E),$$

with $n(E,r_s)$ the density of CRs at the observer's position and $Q(E)$ the emissivity of the source. For quasi-rectilinear propagation $n(E,r_s) \propto r_s^{-2}$, while in the diffusion regime $n(E,r_s) \propto r_s^{-1}$. As a

result of the diffusion process, the spectrum of the flux observed from a given source is modified, with the flux of lower-energy particles being enhanced by an amount that depends on the distance from the observer to the source and on the properties of the magnetic field. We define the enhancement factor ξ as the ratio between the actual density and the one that would result in the case of rectilinear propagation,

$$\xi \equiv \frac{n(E, r_s)}{Q(E)/(4\pi r_s^2 c)} = \frac{1}{\langle \cos\theta \rangle}.$$

We then see that the flux enhancement is inversely proportional to the dipolar component of the flux arriving from the source [20]. Figure 6 shows the enhancement for different distances to the source as a function of E/E_c. At high energies, for which $l_D > r_s$, the propagation is quasi-rectilinear. The enhancement starts at higher energies for farther away sources.

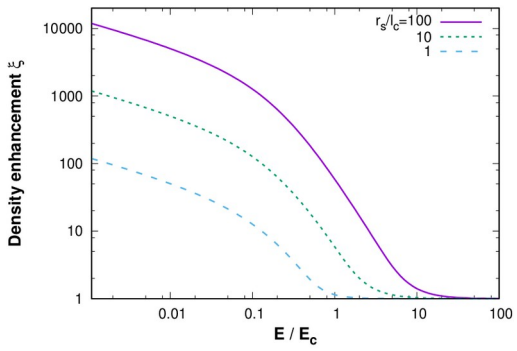

Figure 6: Enhancement of the flux from a single source at a distance r_s due to diffusion [19].

Let us now consider the case of a source emitting CRs since a finite time t_i. In this case a decrease of the flux of the lowest energy particles is expected due to the magnetic horizon effect (MHE). This happens when, due to the diffusive propagation, the time required for low-energy particles to reach the observer becomes larger than the emission time of the source. Figure 7 shows the expected enhancement of the flux for protons accelerated in a source at 4 Mpc for different emission times (left panel). The low-energy suppression of the flux is stronger for the shorter period of emission. The right panel shows the mean cosine angle of CR arrival direction with respect to the source direction. As the emission period decreases, the arrival directions become more concentrated around the source, since only the particles with straighter trajectories have enough time to reach the observer [20].

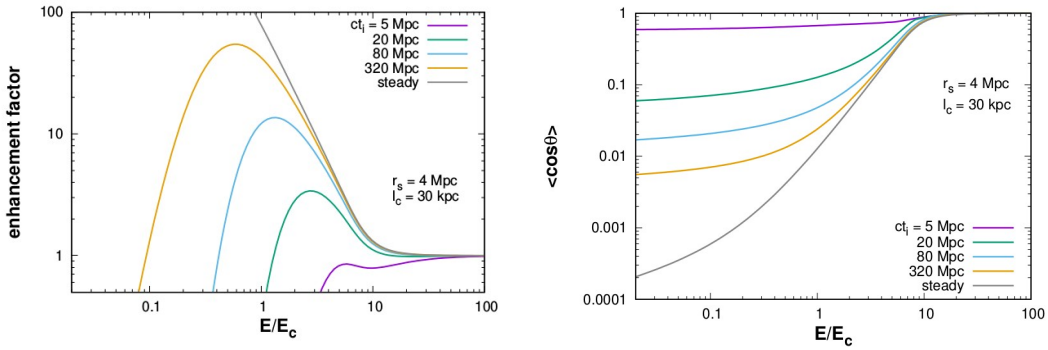

Figure 7: Enhancement of the flux from a single source emitting since t_i (left) and mean cosine angle of the arrival directions with respect to the source location (right).

In the case of a single source emitting protons, there exist an analytic solution for the spectrum of particles in an expanding universe in the diffusive propagation regime [21],

$$n(E) = \int_0^{z_{max}} \mathrm{d}z \left|\frac{\mathrm{d}t}{\mathrm{d}z}\right| Q_s(E_g, z) \frac{\exp\left[-r_s^2/4\lambda^2\right]}{(4\pi\lambda^2)^{3/2}} \frac{\mathrm{d}E_g}{\mathrm{d}E} \qquad \lambda^2(E,z) = \int_0^z \mathrm{d}z' \left|\frac{\mathrm{d}t}{\mathrm{d}z'}\right| \frac{D(E_g, z')}{a^2(z')}$$

where E_g is the energy of the particles emitted by the source and E that of those reaching the observer and the diffusion coefficient is $D = c\, l_D/3$. This solution is shown with a solid line in Fig. 8 for a source at r_s = 36 Mpc emitting protons with a spectrum E^{-2} since a z_{max} = 1 in a turbulent magnetic field with B_{rms} = 1nG with l_c = 1Mpc. At low energies, where particles are propagating diffusively, the solution agrees with the results from numerical simulations represented by dots. At larger energies, for which $l_D(E) \geq r_s$ (in this case $E \approx 3\, E_c \approx 3$ EeV), the propagation becomes ballistic and the spectrum follows that of the emitted particles. At even larger energies, around 100 EeV, photo-pion production by interactions with the cosmic microwave photons leads to the GZK suppression [22,23], with a pileup of higher-energy particles that lost energy through interactions.

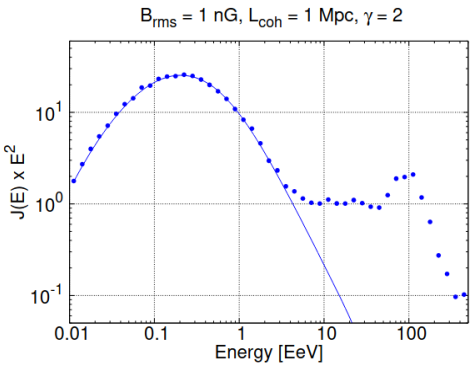

Figure 8: Expected spectrum at Earth from a proton source at 36 Mpc emitting since z_{max}=1 in dots (numerical simulation) and analytical diffusion solution (line).

When multiple sources are present, their fluxes must be summed. A very interesting result, known as the propagation theorem, establishes that as long as the distance to the nearest sources is smaller than the diffusion and the energy loss lengths, the total CR flux is the same as that in the absence of magnetic fields and for a continuous distribution of sources [24]. This can be proved by adding sources, expressing Σ as the integral $\int 4\pi r^2\, \mathrm{d}r$ and using that

$$\int_0^\infty dr\, 4\pi r^2 \exp\left(-r^2/4\lambda^2\right)/\left(4\pi\lambda^2\right)^{3/2} = 1 \quad .$$

4. The magnetic horizon effect

In the case in which the distance to the closest sources is larger than the diffusion length, a suppression of the low-energy particles appears since these have not enough time to reach the observer [25,26,27]. Notice that the relevant magnetic field for this effect is the one in the region between the observer and the closest sources, in our case this most probably corresponds to that within the Local Supercluster. Figure 9 shows in the left panel the modification of the spectrum of protons resulting from the magnetic horizon for different values of the normalized intersource distance $X_s \equiv d_s/\sqrt{R_H L_c} = (d_s/20\,Mpc)\sqrt{100\,kpc/L_c}$, with

R_H the Hubble radius and d_s the mean intersource distance, related to the source density n_s through $n_s = d_s^{-1/3}$. The suppression can be parameterized by a function $G(E/E_c, X_s) = J_Z(E, X_s)/J_Z(E)_{d_s \to 0}$, displayed in the right panel. Larger intersource distances lead to stronger flux suppression.

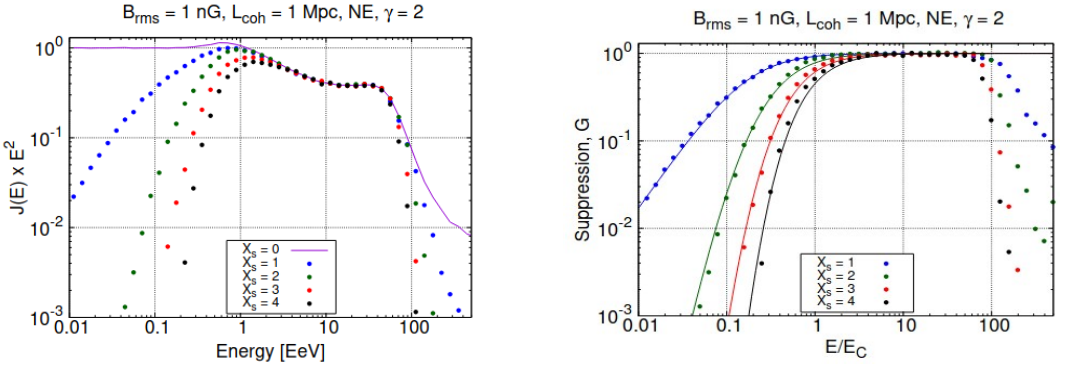

Figure 9: Suppression of the flux for a proton source distribution for different normalized inter-source distances [28].

A similar suppression results for heavier primary nuclei as shown in the left panel of Figure 10. Since the magnetic horizon depends on the rigidity of the particles, the suppression is the same for the different mass groups when plotted as a function of E/E_c as shown in the right panel. Analytic expressions fitting G (solid lines) can be found in [28].

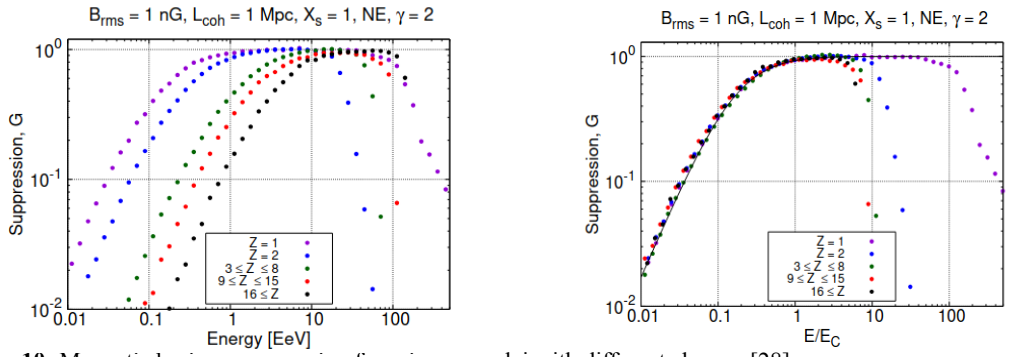

Figure 10: Magnetic horizon suppression for primary nuclei with different charges [28].

Secondary particles produced from the photo-disintegration of heavier nuclei are, however, less suppressed than the primary ones, as can be seen for protons in the left panel of Figure 11. The reason is that they are, on average, produced at higher redshift and have thus a longer time to reach the Earth, as can be seen in the right panel.

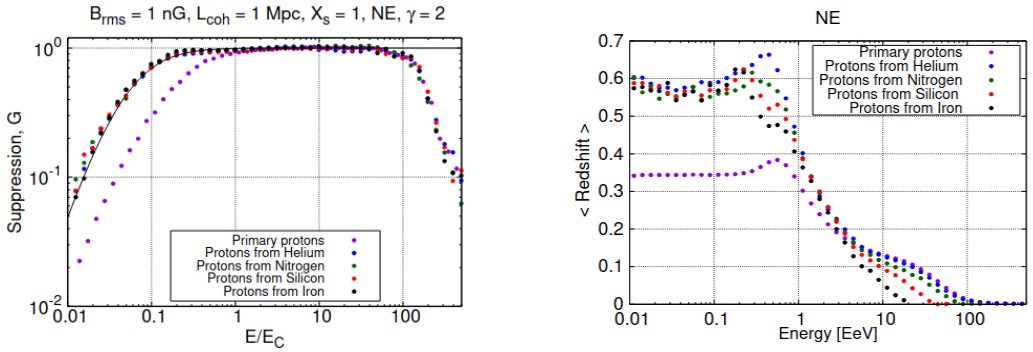

Figure 11: Magnetic horizon suppression for secondary protons [28].

5. Explaing the observed spectrum and composition

The Pierre Auger Observatory performed detailed measurements of the CR spectrum and distribution of the atmospheric depth at the maximum development of the air showers, X_{max}, which is a reliable estimator of the mass composition. These measurements indicate a composition increasingly lighter from 0.6 EeV to 3 EeV, getting progressively heavier above 3 EeV and with little mixing of masses, as shown in the right panel of Fig. 1. These results have been interpreted in scenarios with two populations of uniformly distributed sources accelerating a mixed mass composition of CRs with power-law spectra and rigidity-dependent cutoffs proportional to $\mathrm{sech}(E/ZR_{cut})^{\Delta}$, with the coefficient Δ regulating the steepness of the cutoff [1]. The left panel of Fig. 1 shows the best fit result when considering $\Delta = 1$ and the EPOS-LHC hadronic interaction model for the air-shower development in the atmosphere. This fit requires for the high-energy population a very hard spectrum $E^{2.2}$. The question of whether the hardness of the spectrum of the high-energy population could result from the magnetic horizon effect has been recently analysed by the Pierre Auger Collaboration [2]. A combined fit to the spectrum and X_{max} measurements including the possible MHE for the high-energy population was performed. For a soft cutoff with $\Delta = 1$, the best fit solution was close to the no B case, with a very hard spectrum at the sources, as it is shown in the left panel of Fig. 12 for the Sibyll 2.3d hadronic interaction model. Instead, when a sharper cutoff with $\Delta = 3$ was adopted, the best-fit solution (right panel) corresponds to a significant MHE and a considerably softer spectrum at the source, E^{-2}, compatible with the expectations from the diffusive shock acceleration mechanism. This solution requires a strong extragalactic magnetic field in the region between the Milky Way and the closest sources $(B_{rms}/50\,nG)\sqrt{l_c/100\,kpc}\,(d_s/20\,Mpc)\sim 1-2$. A low-energy component with mixed light to intermediate (p+He+N) mass composition and with a soft $E^{-3.6}$ spectrum is also required to explain the observations above 0.6 EeV.

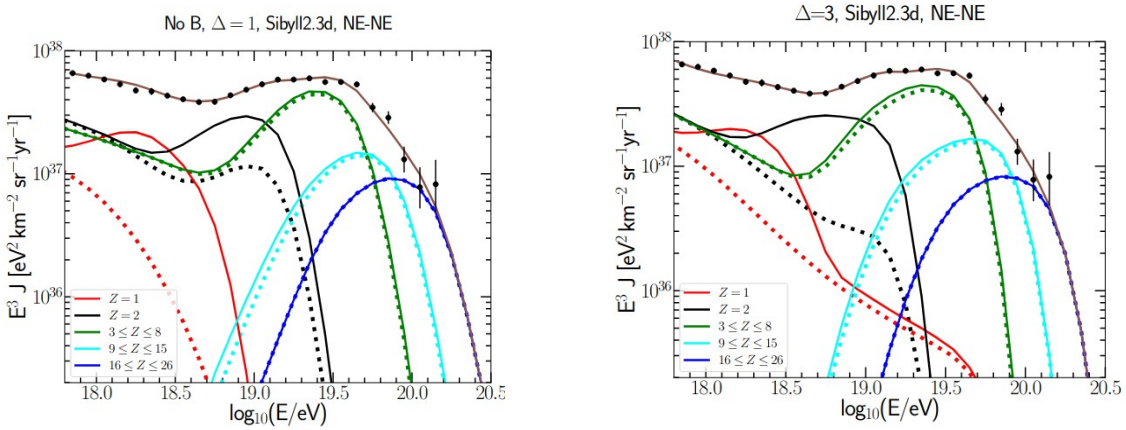

Figure 12: Best fit solution to the spectrum and composition for the Sibyll 2.3d hadronic interactions model and for a soft cutoff $\Delta = 1$ (left) where the fit is close to the no B case and sharp cutoff $\Delta = 3$ (right) with significant MHE [2].

Another possible scenario to explain the observations above the ankle is to consider that the flux is dominated by a single nearby source, like the radio-galaxy Cen A [29]. As discussed in Section 3, for a source emitting CRs since an initial time t_i, the flux reaching an observer at a distance r_s after propagating in a turbulent magnetic field is modified by the factor displayed in the left panel of Fig. 7. A good fit to the spectrum and composition is obtained as shown in Fig.

13 including also a low-energy extragalactic component similar to that of the previous case. The best fit source spectrum for this case is $E^{-1.7}$ and the source started to emit 600 Mly ago. A strong magnetic field of few tens nG between the Milky Way and the nearby source is needed. Note that this will produce a significant blurring of the source, while the Galactic magnetic field can lead to lensing effects and multiple imaging which would spread the arrival distribution of the CRs and leads to a better agreement with the observations [29]. As an example, the expected flux distribution at 10 EeV is shown in the right panel of Fig. 13.

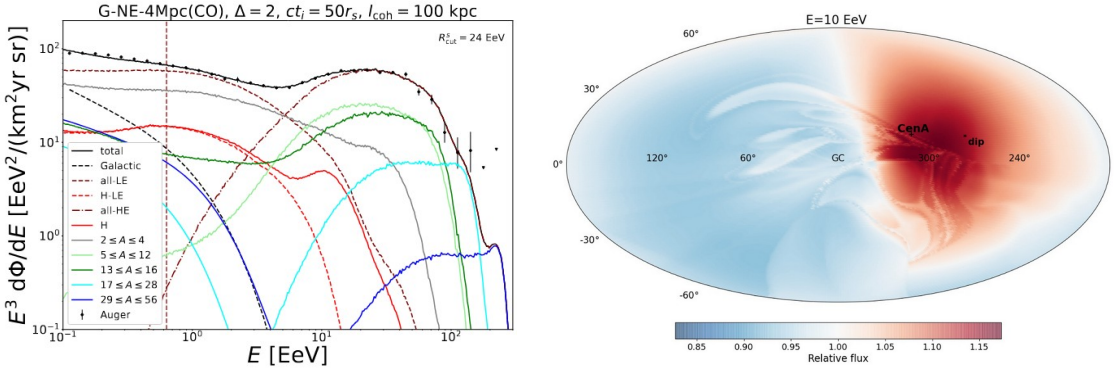

Figure 13: Cen A scenario. Left: contribution to the flux of the different components. Right: distribution of the flux at 10 EeV [29].

5. Dipole expectations

An important measurement is the dipolar anisotropy observed above the ankle energy. It grows with energy from about 2% at 5 EeV to 17% above 32 EeV [3]. This behavior may be attributed to CR energy losses from interactions with background radiation, resulting in a shrinking horizon at higher energies. This is expected to lead to a growing relative contribution from nearby sources, whose distribution is more inhomogeneous, resulting in an increase in the dipole amplitude as a function of energy. It has been shown that the expected dipole from sources following the distribution of galaxies, with a source density of 10^{-5} Mpc^{-3} or 10^{-4} Mpc^{-3}, and emitting according to the model for the high-energy population that fits the spectrum and composition, is consistent with dipole measurements both in amplitude and direction [3].

It is interesting to discuss the effect that a turbulent extragalactic magnetic field has on the dipolar anisotropy in the case of a distribution of CR sources, extending the discussion of the single source case presented in Section 3. The total dipole is given by the vectorial sum of the dipoles from each individual source,

$$\vec{\Delta}(E) = \sum_{i,j} \frac{n_i^{(j)}(E)}{n_t(E)} \vec{\Delta}_i^{(j)}(E),$$

where the index i runs over the sources and j over the mass groups contributing to the flux. The dipole of the mass group j and from the source i points to the source direction $\hat{n}_i$ and has an amplitude equal to $\vec{\Delta}_i^{(j)} = 3\langle \cos\theta_i^{(j)} \rangle \hat{n}_i$, and thus decreases for increasing spreading of the arrival direction of the diffusing particles. Each individual dipole has to be weighted by the relative contribution of that source and mass group to the total flux, $n_i^{(j)}/n_t$. As we have discussed in Section 3, when CRs propagate diffusively in the presence of a turbulent field

there is an enhancement in the density, that for steady sources (and neglecting energy losses) is inversely proportional to the decrease in the dipole amplitude, $n_i^{(j)} = Q_i^{(j)} / \left(4\pi r_i^2 \langle \cos\theta_i^{(j)} \rangle\right)$, with $Q_i^{(j)}$ the emissivity of source i of particles in the mass group j. Then, the product

$$n_i^{(j)} \vec{\Delta}_i^{(j)} = \frac{3 Q_i^{(j)}}{4\pi r_i^2} \hat{n}_i$$

is the same in the presence or in the absence of the turbulent magnetic field. We see that the effects of the dipole dilution and the flux enhancement compensate each other in this ideal case. Then, as long as n_t is not affected by the extragalactic turbulent magnetic field (i.e. the propagation theorem holds), the total dipolar component of the anisotropy is nearly independent of the field strength. This cancellation only applies for the dipole, while smaller scale anisotropies are instead affected by the EGMF. The independence of the dipole amplitude from the magnitude of the turbulent magnetic field present also holds to a good approximation in the more realistic case in which the interactions with the radiation backgrounds are taken into account, as shown in the left panel of Fig. 14 [18].

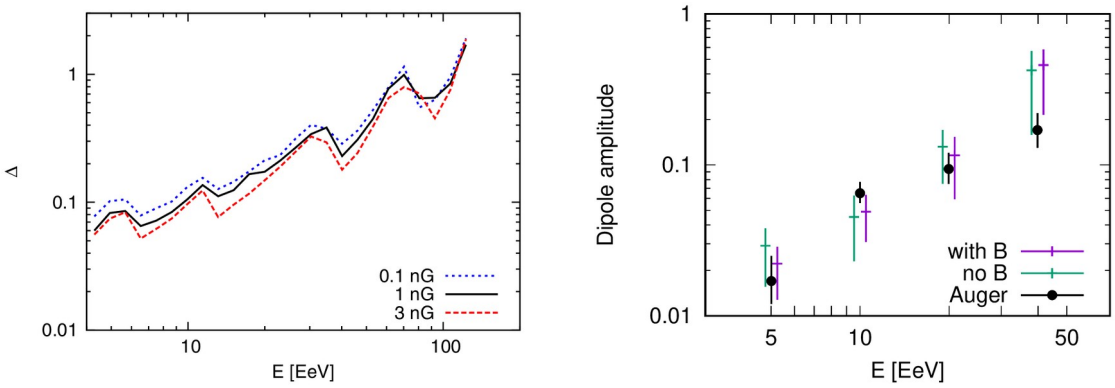

Figure 14: Left: dipolar anisotropy for a uniform distribution of sources with spatial density of 10^{-5} Mpc^{-3} for the model of ref. [18] and different amplitudes of the turbulent field. Right: Dipole amplitude for the model with MHE (right panel of Fig. 12) presented in Section 4, for sources distributed like galaxies and a density 10^{-4} Mpc^{-3} and a turbulent field with $B_{\rm rms}$ = 50 nG and l_c= 25 kpc.

Also when larger turbulent magnetic fields are considered, such as those leading to a strong MHE effect discussed in Section 4, the dipole amplitude is only mildly affected, as shown in the right panel of Fig.14. The expected dipole amplitude for the best fit model of spectrum and composition depicted in the right panel of Fig. 12, considering sources distributed like galaxies and with a density of 10^{-4} Mpc^{-3}, is very similar when a strong magnetic field of 50 nG is included in the simulations and in the no magnetic field case. Let us note that the expected amplitude also agrees well with the measurements of the Pierre Auger Collaboration [3].

6. Summary

Galactic and extragalactic magnetic fields likely significantly affect the flux of cosmic rays reaching Earth, even at the highest observed energies, influencing both arrival directions (and thus observed anisotropies) and the spectrum.

The regular magnetic field deflects the cosmic-ray trajectories by an amount inversely proportional to their rigidity, and thus could lead to sets of events ordered in energy in the sky

along a preferred direction, although this has not yet been detected. Another interesting effect resulting from the regular GMF is the possibility of multiple images of one source, that is CRs from the same direction outside the halo can arrive to the Earth following very different trajectories. Given the inferred heavy composition at the highest energies, with corresponding rigidities below 4 – 5 EV, this is expected to happen for certain directions of the sky up to the maximum observed energies, complicating the identification of CR sources. The Galactic magnetic field also significantly affects the large-scale anisotropies, in particular the direction of the dipolar component of the flux reaching the Earth is rotated towards a direction closer to the spiral arm direction and its amplitude is reduced compared to that outside the halo.

Turbulent magnetic fields blur the image of a single source; this blurring increases with distance and decreases with energy, resulting in a weaker dipolar flux component from the source. At the same time, the diffusion of CRs leads to an enhancement of the flux that for steady sources is inversely proportional to the dipole decrease. For a source emitting since a finite time the spectrum is suppressed at low energies due to the magnetic horizon effect.

On the other hand, the flux of particles from a distribution of many sources is not affected by the turbulent magnetic field as long as the diffusion length is larger than the average intersource distance. When this is not the case, a depletion of the total flux at low energies appears. This has been proposed as a possible explanation for the observed hardness of the spectrum of the high-energy extragalactic CR component.

Another scenario that provides a good fit to the spectrum and composition measurements at the highest energies is that of a local dominant source emitting since a limited time.

In summary, several possible scenarios explain the observations, and understanding the effects of cosmic magnetic fields is key to their study.

References

[1] Pierre Auger Collaboration, *Constraining the sources of ultra-high-energy cosmic rays across and above the ankle with the spectrum and composition data measured at the Pierre Auger Observatory, JCAP* **05** (2023) 024 [arXiv:2211.02857]

[2] Pierre Auger Collaboration, *Impact of the magnetic horizon on the interpretation of the Pierre Auger Observatory spectrum and composition data*, *JCAP* **07** (2024) 094 [arXiv:2404.03533]

[3] Pierre Auger Collaboration, *Large-scale Cosmic-ray Anisotropies with 19 yr of Data from the Pierre Auger Observatory*, *ApJ* **976** (2024) 48 [arXiv:2408.05292]

[4] Pierre Auger Collaboration, *Arrival Directions of Cosmic Rays above 32 EeV from Phase One of the Pierre Auger Observatory, ApJ* **935** (2022) 170 [arXiv:2206.13492]

[5] F. Vazza et al., *Simulations of extragalactic magnetic fields and of their observables. Class. Quantum Gravity* **34** (2027) 234001

[6] M. Haverkorn, *Magnetic Fields in the Milky Way, in Magnetic Fields in Diffuse Media, Astrophysics and Space Science Library* **407**, Springer (2015) 483 [arXiv:1406.0283]

[7] M. Unger, *The Galactic Magnetic Field and its Uncertainties*, these proceedings

[8] A. Korochkin, *New model of the coherent magnetic field the Milky Way and UHECR propagation,* these proceedings

[9] J. P. Vallée, *Magnetic fields in the galactic Universe, as observed in supershells, galaxies, intergalactic and cosmic realms, New Astron. Rev.* **55** (2011) 91

[10] F. Vazza et al., *Magnetogenesis and the Cosmic Web: A Joint Challenge for Radio Observations and Numerical Simulations, Galaxies* **9** (2021) 109

[11] R. Jansson and G. R. Farrar, *A new model of the galactic magnetic field, ApJ* **757** (2012) 14

[12] D. Harari, S. Mollerach and E. Roulet, *The toes of the ultra high energy cosmic ray spectrum, JHEP* **08** (1999) 022

[13] Pierre Auger Collaboration, *Search for magnetically-induced signatures in the arrival directions of ultra-high-energy cosmic rays measured at the Pierre Auger Observatory, JCAP* **06** (2020) 017

[14] S. Mollerach and E. Roulet, *Anisotropies of ultrahigh-energy cosmic rays in a scenario with nearby sources*, *Phys Rev D* **105** (2022) 6

[15] Pierre Auger Collaboration, *Large-scale Cosmic-Ray Anisotropies above 4 EeV Measured by the Pierre Auger Observatory, ApJ* **868** (2018) 4

[16] D. Harari, S. Mollerach and E. Roulet, *Anisotropies of ultrahigh energy cosmic rays diffusing from extragalactic sources, Phys Rev D* **89** (2014) 123001

[17] A. Achterberg et al., *Intergalactic Propagation of UHE Cosmic Rays* [astro-ph/9907060]

[18] D. Harari, S. Mollerach and E. Roulet, *Anisotropies of ultrahigh energy cosmic ray nuclei diffusing from extragalactic sources, Phys Rev D* **92**(2015) 063014

[19] D. Harari, S. Mollerach and E. Roulet, *Angular distribution of cosmic rays from an individual source in a turbulent magnetic field, Phys Rev D* **93** (2016) 6

[20] S. Mollerach and E. Roulet, Ultrahigh energy cosmic rays from a nearby extragalactic source in the diffusive regime, *Phys Rev D* **99** (2019) 103010

[21] V. Berezinsky and A.Z. Gazizov, *Diffusion of Cosmic Rays in the Expanding Universe 1, ApJ* **643** (2006) 8

[22] K. Greisen, *End to the Cosmic-Ray Spectrum?, Phys Rev Lett* **16** (1966) 748

[23] G.T. Zatsepin and V.A. Kuzmin, *Upper limit of the spectrum of cosmic rays, JETP Lett.* **4** (1966) 78

[24] R. Aloisio and V. Berezinsky, *Diffusive propagation of UHECR and the propagation theorem, ApJ* **612** (2004) 900 [astro-ph/0403095]

[25] V. Berezinsky and A.Z. Gazizov, *Diffusion of Cosmic Rays in the Expanding Universe. 2. Energy Spectra of Ultra-High Energy Cosmic Rays, ApJ* **669** (2007) 684 [astro-ph/0702102]

[26] M. Lemoine, *Extra-galactic magnetic fields and the second knee in the cosmic-ray spectrum, Phys Rev D* **71** (2005) 083007 [astro-ph/0411173]

[27] D. Allard, *Extragalactic propagation of ultrahigh energy cosmic-rays, Astrop. Phys.* **39** (2012) 33

[28] J.M. González, S. Mollerach and E. Roulet, *Magnetic diffusion and interaction effects on ultra-high energy cosmic rays: Protons and nuclei, PRD* **104** (2021) 063005 [arXiv:2105.08138]

[29] S. Mollerach and E. Roulet, *Case for Centaurus A as the main source of ultrahigh-energy cosmic rays*, *Phys Rev D* **110** (2024) 6.